ISBN: 978-3-95450-132-8 doi:10.18429/JACoW-IPAC2014-TUPRI045

BEAM COUPLING IMPEDANCE SIMULATION IN THE FREQUENCY DOMAIN FOR THE SIS100 SYNCHROTRON *

U. Niedermayer† and O. Boine-Frankenheim
Technische Universität Darmstadt, Institut für Theorie Elektromagnetischer Felder (TEMF),
Schlossgartenstraße 8, 64289 Darmstadt, Germany

Abstract

For the quantification of intensity thresholds due to coherent instabilities and beam induced heating in the FAIR synchrotron SIS100 a detailed knowledge of transverse and longitudinal beam coupling impedance is required. Due to the rather long proton and heavy-ion bunches, the relevant spectrum is below 100MHz. For the computation of beam coupling impedances in the low frequency regime, frequency domain methods are more advantageous than (explicit) time domain methods. We show the setup of a 2D finite element code that allows to compute the impedance for arbitrary longitudinally homogeneous beam and structure shapes. Perfectly conducting pipes, a dispersive ferrite tube, and thin resistive beam pipe serve as test cases. The influence of the beam velocity on the coupling impedance is studied.

INTRODUCTION

The beam in a synchrotron is modeled as a disc with radius a and surface charge density σ traveling with velocity βc. The displacement d_x of the beam (i.e. a coherent dipole oscillation) can be approximated to first order by

$$\sigma(\varrho,\varphi) \approx \frac{q}{\pi a^2}(\Theta(a-\varrho) + \delta(a-\varrho)d_\mathrm{x}\cos\varphi). \quad (1)$$

The force acting back on the beam is described by the coupling impedance [1]

$$\underline{Z}_\parallel(\omega) = -\frac{1}{q^2}\int_\mathrm{beam} \underline{\vec{E}}\cdot\underline{\vec{J}}^*_\parallel \mathrm{d}V \quad (2)$$

$$\underline{Z}_{\perp,\mathrm{x}}(\omega) = -\frac{\beta c}{(q d_\mathrm{x})^2\omega}\int_\mathrm{beam} \underline{\vec{E}}\cdot\underline{\vec{J}}^*_\perp \mathrm{d}V. \quad (3)$$

where the beam current in frequency domain (FD) is obtained from Eq. 1 as

$$\underline{J}_{\mathrm{s,z}}(\varrho,\varphi,z;\omega) = \underline{J}_\parallel + \underline{J}_\perp = (\sigma_\parallel + \sigma_\perp)e^{-i\omega z/\beta c} \quad (4)$$

such that its magnitude is independent of the beam velocity.

The task is to solve Maxwell's equations subject to excitation by $\underline{J}_{\mathrm{s,z}}$, including the charge that can be obtained by the continuity equation. This has been approached by the Finite Integration Technique (FIT) as described in [2] and references therein. Nonetheless, straightforward implementations of staircase FIT suffer from slow convergence on curved surfaces. This paper will focus on the Finite Element Method (FEM) in 2D on a standard unstructured triangular mesh. The algorithm is implemented using FEniCS [3, 4], an automated FEM toolbox providing a 'Functional Analysis' framework. The mesh originates from GMSH [5] and is imported using DOLFIN-CONVERT [6]. FEniCS does not provide complex functions, but it is easily possible to define coupled function spaces. This motivates splitting real and imaginary parts and solving the coupled problem, which should have the same number of degrees of freedom (dofs) as the complex problem.

2D IMPEDANCE FEM SOLVER

The fields required to determine the coupling impedance are solutions of

$$\nabla\times\underline{\nu}\nabla\times\underline{\vec{E}} - \omega^2\underline{\varepsilon}\,\underline{\vec{E}} = -i\omega\underline{\vec{J}}_\mathrm{s} \quad (5)$$

with the complex reluctivity $\underline{\nu} = \underline{\mu}^{-1} = (\mu' + i\mu'')/|\mu|^2$, and the complex permittivity $\underline{\varepsilon} = \varepsilon_0\varepsilon_r - i\kappa/\omega$ (conductivity κ) as functions of position and frequency. On the sufficiently smooth boundary $\partial\Omega$ of the computational domain $\Omega \subset \mathbb{R}^2$ a Dirichlet condition, i.e. $\vec{n}\times\underline{\vec{E}}|_{\partial\Omega} = 0$, is applied. Therefore, for brevity, all boundary terms in weak formulations are omitted. The Fourier correspondence $\partial_z \to -i\omega/v$ motivates splitting the electric field as

$$\underline{\vec{E}} = \begin{pmatrix} \vec{E}^\mathrm{r}_\perp \\ E^\mathrm{r}_z \end{pmatrix} + i\begin{pmatrix} \vec{E}^\mathrm{i}_\perp \\ E^\mathrm{i}_z \end{pmatrix} \quad (6)$$

where the upper incices denote real and imaginary parts. In order to avoid 'too much continuity' on material interfaces, Nedelec edge-elements [7] are used for the vectorial part of the fields. Since they are H(curl) conformal, the divergence part is calculated separately by applying a Helmholtz split $\underline{\vec{E}} = \underline{\vec{E}}_\mathrm{curl} + \underline{\vec{E}}_\mathrm{div}$. For $\underline{\vec{E}}_\mathrm{div} = -\nabla\underline{\Phi}$ the Poisson equation

$$\nabla\cdot\underline{\varepsilon}\nabla\underline{\Phi} = -\underline{\varrho} = -\frac{1}{\beta c}\underline{J}_{\mathrm{s,z}} \quad (7)$$

has to be solved and for the rotational part the same curlcurl equation as Eq. 5,

$$\nabla\times\underline{\nu}\nabla\times\underline{\vec{E}}_\mathrm{curl} - \omega^2\underline{\varepsilon}\,\underline{\vec{E}}_\mathrm{curl} = \underline{\vec{R}}, \quad (8)$$

is found, but with a divergence free right hand side

$$\underline{\vec{R}} = \omega^2\underline{\varepsilon}\,\underline{\vec{E}}_\mathrm{div} - i\omega\underline{\vec{J}}_s. \quad (9)$$

Statics Solver

Equation 7 represents a coupled electrostatic and stationary current problem

$$\begin{aligned}\nabla\cdot\varepsilon\nabla\Phi^\mathrm{r} + \nabla\cdot\frac{\kappa}{\omega}\nabla\Phi^\mathrm{i} &= -\varrho^\mathrm{r}\\ \nabla\cdot\varepsilon\nabla\Phi^\mathrm{i} - \nabla\cdot\frac{\kappa}{\omega}\nabla\Phi^\mathrm{r} &= -\varrho^\mathrm{i}.\end{aligned} \quad (10)$$

* Work supported by GSI Darmstadt
† u.niedermayer@gsi.de

ISBN: 978-3-95450-132-8 doi:10.18429/JACoW-IPAC2014-TUPRI045

It is solved by standard Galerkin FEM 1st order nodal trial- and test-functions

$$\Phi^{\mathrm{r}} = \sum_{k=1}^{N_{\mathrm{n}}} a_k^{\mathrm{r}} N_k(x,y) \tag{11}$$

The electric field on a mesh edge j is obtained by $\vec{E}^{\mathrm{r}}_{\perp,j} = -\nabla_\perp \Phi^r = (\Phi^{\mathrm{r}}_{k'} - \Phi^{\mathrm{r}}_k)\vec{t}_j/l_j$, which is then projected on the H(curl) basis.

Curlcurl Solver

In order to solve Eq. 8 we decompose the curl operator as

$$\nabla \times \underline{\vec{E}} = \left(\begin{array}{cc|c} 0 & -\partial_z & \partial_y \\ \partial_z & 0 & -\partial_x \\ \hline -\partial_y & \partial_x & 0 \end{array}\right) \underline{\vec{E}} = \left(\begin{array}{c|c} iZ & A \\ \hline B & 0 \end{array}\right) \underline{\vec{E}} \tag{12}$$

$$Z^2 = -\frac{\omega^2}{\beta^2 c^2} I \quad , \quad A = -B^T \tag{13}$$

such that the stiffness term in the weak formulation

$$\int_\Omega \nabla \times \nu^r \nabla \times \vec{E}^r_{\mathrm{curl}} \cdot \begin{pmatrix} \vec{w}_k \\ \nu_l \end{pmatrix} \mathrm{d}\Omega \tag{14}$$

can be assembled using

$$\int_\Omega (A\nu^{\mathrm{r}} B\vec{E}^{\mathrm{r}}_\perp) \cdot \vec{w}^{\mathrm{r}}_j \mathrm{d}\Omega = \int_\Omega (\nu^{\mathrm{r}} B\vec{E}^{\mathrm{r}}_\perp)(B\vec{w}^{\mathrm{r}}_j)\mathrm{d}\Omega \tag{15}$$

$$\int_\Omega (B\nu^r AE^{\mathrm{r}}_z)\nu^{\mathrm{r}}_j \mathrm{d}\Omega = \int_\Omega (\nu^{\mathrm{r}} AE^{\mathrm{r}}_z) \cdot (A\nu^{\mathrm{r}}_j)\mathrm{d}\Omega. \tag{16}$$

Finally, a Galerkin approach with 1st order reduced Nedelec elements (see also e.g. [8])

$$\vec{E}^r_\perp(\vec{x}) = \sum_{i=1}^{N_{\mathrm{e}}} e^r_i \vec{w}_i(\vec{x}) \tag{17}$$

$$\vec{w}_i(\vec{x}) = N_k \nabla N_l - N_l \nabla N_k \tag{18}$$

is applied, fulfilling

$$\int_{l_j} \vec{w}_i \cdot \vec{t}_j \mathrm{d}s = \delta_{ij}. \tag{19}$$

For brevity we skip the explicit form of the complete curl-curl stiffness operator containing 20 terms, the mass operator containing 8 terms and the linear form for $\underline{\vec{R}}$ containing 4 terms. The total number of dofs at lowest order is $2 * (\#edges + \#nodes)$, as expected from Eq. 6, plus $2 * \#nodes$ of the Poisson system.

SELECTED BENCHMARK EXAMPLES

When the relativistic velocity is $\beta < 1$, the solution of Eq. 5 always contains a space charge part, i.e. an impedance due to interaction of the source with itself and with image charges. For structures with largely varying skin-depth it cannot be separated from the resistive wall impedance. Therefore, the code is first validated with a uniform cylindrical perfectly conducting (PEC) pipe. Subsequently, the code is applied to a thin resistive pipe and a dispersive Ferrite ring.

Space Charge Impedance

The longitudinal and transverse space charge impedance is calculated for a uniform cylindrical beam and pipe of radius $a = 0.01$m and $b = 0.04$m, respectively. The results

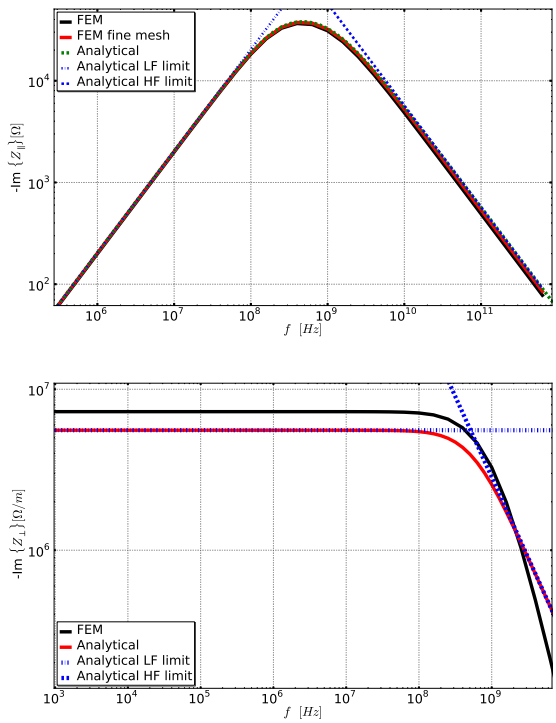

Figure 1: Longitudinal and transverse space charge impedance for uniform cylindrical beam and PEC pipe for $\beta = 0.1$ ($l = 1$m)

can be seen in Fig. 1, where the asymptotes are

$$\underline{Z}^{\mathrm{spch}}_{\parallel,\mathrm{LF}} = \frac{-i\omega\mu_0 lg}{2\pi\beta^2\gamma^2} \ , \quad g = \frac{1}{4} + \ln\frac{b}{a} \ , \quad \underline{Z}^{\mathrm{spch}}_{\parallel,\mathrm{HF}} = \frac{-il}{\omega\varepsilon_0\pi a^2}$$

$$Z^{\mathrm{spch}}_{\perp,\mathrm{LF}} = \frac{-iZ_0 l}{2\pi\beta\gamma^2}\left(\frac{1}{a^2} - \frac{1}{b^2}\right) \ , \quad \underline{Z}^{\mathrm{spch}}_{\perp,\mathrm{HF}} = \frac{-ilZ_0 c}{2\pi a^3\gamma\omega} \tag{20}$$

and the full analytical solutions can be found in [1]. The discrepancy in the transverse impedance originates from improper representation of the dipole moment on the FEM mesh, i.e. a linear function has been used instead of the δ-function in Eq. 1, $\sigma_\perp = x\sigma_\parallel$, leading to improper scaling with a.

Resistive Beam Pipe

Figure 2 shows the resistive wall impedance for the same pipe inner radius but 1mm thickness, finite conductivity $\kappa = 10^6$S/m, and radius of the boundary 0.1m. The analytical result was obtained by ReWall [9]. A major problem in the FEM simulation is to resolve the skin depth, which becomes very small at HF. This can be eased by using surface impedances or sophisticated thin sheet approaches (see e.g. [10]), or as done here by refining the mesh. Note that a very fine mesh at LF can lead to numerical instability, which requires adapting the mesh according to frequency and β.

ISBN: 978-3-95450-132-8 doi:10.18429/JACoW-IPAC2014-TUPRI045

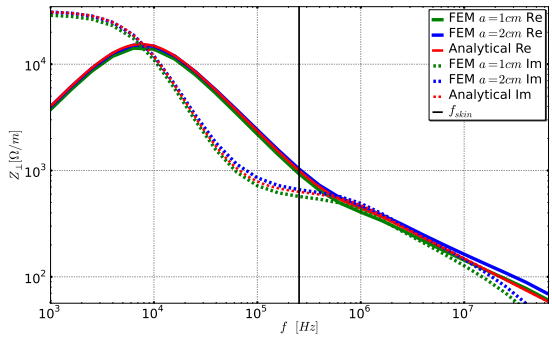

Figure 2: $Z_\perp$ of a resistive pipe for $\beta = 1$ ($l = 1$m).

Dispersive Ferrite Ring

The last example is a ring of Ferrite Amidon43 [11] (see Fig. 3) which has strongly dispersive material properties. Therefore geometric resonances are not visible in the impedance and one observes a broadband peak. Figure 4

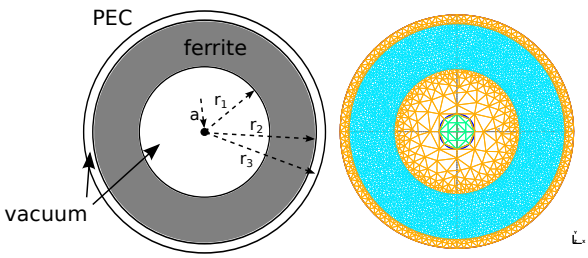

Figure 3: Ferrite ring geometry and mesh, $a = 0.5$cm, $r_1 = 1.78$cm , $r_2 = 3.05$cm , $r_3 = 3.3$cm , $l = 2.54$cm.

shows the β dependence of the impedance. The analytical results are obtained by a field-matching implementation in Mathematica [12], similar to the one in [13].

CONCLUSION AND OUTLOOK

For longitudinal impedances the presented 2D solver works very well, arbitrary beam and structure shapes can be simulated for a large range of β and frequency. Problems occur only for extremely small longitudinal impedance, such as the resistive wall impedance at frequencies below the image current onset (see also [13]). Transverse impedances are more complicated to compute, since the dipole moment cannot be represented as in Eq.1. Nonetheless, satisfactory results have been obtained for rather large beam radius a. This code is particularly well suited for low β, since β enters only as a parameter. Nonetheless the mesh requirements depend on β via the transverse wavenumber. Note that for dispersive material the frequency dependence of the speed of light has to be taken into account in the choice of the mesh. For checking the the 2D assumption a 3D code is required which is presently under development.

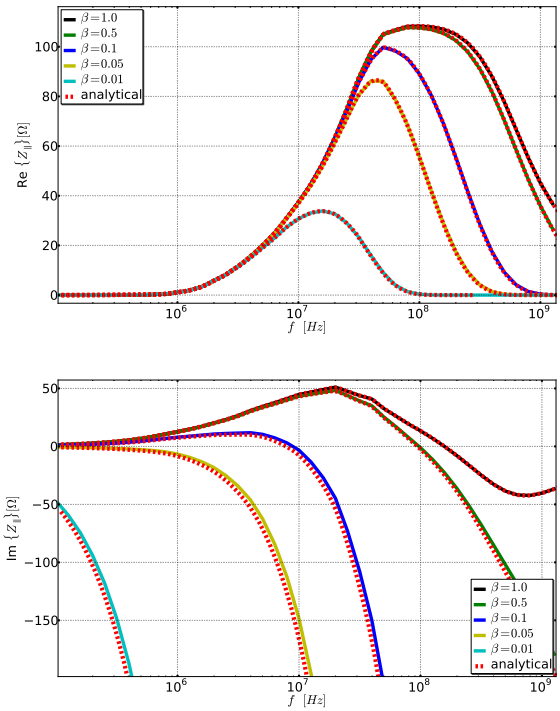

Figure 4: Longitudinal impedance of a ferrite ring.

REFERENCES

[1] R. Gluckstern, Cern Accelerator School, 2000.

[2] U.Niedermayer and O. Boine-Frankenheim, Proc. of ICAP, 2012.

[3] A. Logg, K.-A. Mardal, G. N. Wells et al. , Automated Solution of Differential Equations by the Finite Element Method, Springer, 2012.

[4] `www.fenicsproject.org`

[5] C. Geuzaine and J.-F. Remacle, GMSH 2.8.4, `www.geuz.org/gmsh`, 2014.

[6] A. Logg, DOLFIN-CONVERT, `www.people.sc.fsu.edu/~jburkardt/py_src/dolfin-convert/dolfin-convert.html`, 2010.

[7] J.C. Nedelec, Numer. Math. 35, 315-341 (1980).

[8] P. Ingelström, IEEE Trans. MTT Vol. 54 No. 1, 2006.

[9] N. Mounet and E. Metral, CERN-BE-2009-039, see also `www.cern.ch/imp`

[10] K. Schmidt and A. Chernov, SIAM J. Appl. Math., 73(6), 2013.

[11] Amidon Material 43, `http://www.amidon.de/contents/de/d542.html`

[12] Wolfram *Mathematica 9.0®*,`www.wolfram.com`, 2013.

[13] U. Niedermayer and O. Boine-Frankenheim, NIM A 687, 51-61, 2012.